Numerical simulation of low aspect ratio fixed wings for MAV applications

M.B.Subrahmanya[1] *D.S.Kulkarni* [1] *B.N.Rajani*[1]

[1]*CTFD Division, NAL (CSIR), Bangalore 560 017, India (email:rajani@ctfd.cmmacs.erent.in)*

Corresponding author ***B.N.Rajani***

Abstract :

Turbulent flow past low aspect ratio (AR) thin wing with two different planform shapes *viz.*, rectangular and inverse Zimmerman has been carried out at a Reynolds number $(Re)=2.4\times10^5$ to analyze their aerodynamic characteristics using the Unsteady Reynolds Averaged Navier Stokes (URANS) equations coupled to k-ε turbulence model. In the present work the aerodynamic characteristics of thin wings with different planforms are studied and the three dimensional effects which are prominent in low AR are also discussed by comparing with 2D simulations carried out for the root section of the wing.

Keywords: *Mulitiblock Finite volume solver, Low Re flow, k-ε turbulence model, inverse Zimmerman planform, Low aspect ratio wing*

1. Introduction

Micro Air Vehicles (MAV) are unmanned autonomous aircraft, with a maximal size of 30 cm and flight speed around 14 m/s with 30 minute endurance and weighing below 300 g have gained interest from both military and civilian community. A single MAV or a swarm of MAVs can be used effectively to measure or gather data in hostile environments, for surveillance in urban and confined spaces, and provide situational awareness in a battlefield scenario. In order to gather reliable data, these MAVs need to have ability to loiter for a long duration and also have an efficient maneuver capability both in open and confined space. During last decade significant progress has been made in this field, however no vehicle has been able to achieve a long loiter time or have an efficient maneuverability with proper navigational guidance. Several factors which contributed to this poor performance are lack of understanding of aerodynamics, structural mechanics and the propulsion system at the micro scale and also the inadequate knowledge on the visual guidance and navigation systems. On the other hand in nature, biological fliers like insects and small birds with a small brain and a limited processing capacity, have evolved like miniature flying machines which efficiently perform far more difficult missions compared to those achieved by MAVs. This superior performance may be attributed to three factors: ability to generate lift more efficiently than the existing technologies, ability to store and release energy efficiently and superior mechanisms of visual guidance and navigation.

The small length and the low velocity resulting in a flight regime with a very low Reynolds number ($10^4 < Re < 5 \times 10^5$) pose challenges in aerodynamic design of MAVs. Aerodynamic design of MAVs, reported so far, have employed different kinds of efficient lift generation systems viz., fixed wing [1,2,3], flapping wings [4], flexible wing [5] and rotary wings [6] and or their combinations. The fixed-wing MAVs are commonly used because they are simple and easy to implement and they usually fly at the upper end of the low Reynolds number regime around 5×10^5 [7]. The growing interest in MAVs and their aerodynamic challenges have created the need for improved understanding of the aerodynamics and related flow physics. It is well known from literature [3,7,8] that at low Reynolds number, the aerodynamic characteristics greatly depend on the aerofoil geometry. In general the MAVs require aerofoil with small thickness and significant camber in order to have a better aerodynamic performance at low Reynolds number. Furthermore the small dimension of MAV

demand wing with low aspect ratio. Recent research [1,7] has shown that wing planforms which are rectangular, elliptical, circular or its variants are ideal for MAV application since they offer more lifting area. The present paper focuses on the 3D numerical simulation of turbulent flow past thin wing with two different planform shapes viz., rectangular and inverse Zimmerman (formed by joining two half-ellipses at the three-quarter chord location) at $Re=2.4\times10^5$. The major complexity at low Reynolds number is that the flow is transitional which is computationally difficult to handle [2,3]. The phenomenon of transition from laminar to turbulent flow is not well understood and none of the presently available turbulence models can accurately simulate this complex phenomenon. However for the present relative performance study the flow is assumed to be fully turbulent and the k-ε model has been used to simulate the turbulence.

2. Finite Volume Method

2.1 Governing equations

The phase-averaged Navier Stokes equation for unsteady turbulent incompressible flow may be written in non-orthogonal curvilinear coordinates with cartesian velocities as dependent variables in a compact form as follows:

Momentum transport for the cartesian velocity component $\langle U_i \rangle$:

$$\frac{\partial\left(\rho\langle U_i\rangle\right)}{\partial t}+\frac{1}{J}\frac{\partial}{\partial x_j}\left[\left(\rho\langle U_iU_k\rangle\beta_k^j\right)\right]+\frac{1}{J}\frac{\partial}{\partial x_j}\left[-\frac{\mu}{J}\left(\frac{\partial\langle U_i\rangle}{\partial x_m}B_m^j+\frac{\partial\langle U_k\rangle}{\partial x_m}\beta_i^m\beta_k^j\right)\right]+\frac{1}{J}\frac{\partial}{\partial x_j}\left[\langle P\rangle\beta_i^j-\rho\langle u_iu_k\rangle\beta_k^j\right]=S_{U_i} \tag{1}$$

where, $\langle P\rangle$ and $\langle U_i\rangle$ are the phase averaged pressure and velocity components along i direction respectively, μ is the fluid viscosity, B_k^j and β_k^j are the metric coefficients due to transformation from cartesian to curvilinear coordinates and J is the Jacobian of the transformation matrix. u_i is the fluctuating velocity components and S_{U_i} is any momentum source other than the pressure gradient. These momentum equations are further supplemented by the mass conservation or the so-called continuity equation.

Mass conservation (Continuity):

$$\frac{\partial}{\partial x_j}\left(\rho\langle U_k\rangle\beta_k^j\right)=0 \tag{2}$$

However the above Eqs. 1 and 2 do not form a closed system due to the presence of the unknown turbulent stress term, $-\rho\langle u_iu_j\rangle$

2.2 Turbulence modeling

In eddy viscosity based turbulence models, the turbulent stress appearing in the Reynolds-Averaged equations is expressed in terms of the mean velocity gradients as following:

$$-\rho\langle u_iu_j\rangle=\mu_t\left(\frac{\partial\langle U_i\rangle}{\partial x_j}+\frac{\partial\langle U_j\rangle}{\partial x_i}\right)-\frac{1}{3}\rho\delta_{ij}\langle u_mu_m\rangle \tag{3}$$

where, δ_{ij} is the Kronecker delta and m is the summing index over m = 1, 2, 3. The term $\frac{2}{3}\rho k\delta_{ij}$ only ensures that the sum of the normal stresses is $2k$ as per the definition of k, the turbulent kinetic energy $k=\frac{1}{2}\overline{u_iu_j}$. The eddy viscosity μ_t is assumed to be an isotropic scalar quantity whose value depends on the local state of turbulence. For the present work standard k-ε model [9] is used to simulate the turbulence.

2.3 Numerical solution of finite volume equation

The present computation has been carried out using the in-house multi-block structured RANS (Reynolds Averaged Navier Stokes) code RANS3D [10, 11] developed at the CTFD Division, NAL Bangalore. This code is based on an implicit finite volume algorithm to solve the time averaged Navier-Stokes equation for unsteady incompressible turbulent flow coupled to a wide spectrum of state-of-the-art eddy viscosity based turbulence models. Further this code uses central difference and other higher order upwind schemes for spatial discretization of the convective fluxes and second order accurate three-level fully implicit scheme for temporal discretization. An iterative decoupled approach similar to the SIMPLE algorithm [12], modified for collocated variable arrangement [13] is adopted to avoid the checkerboard oscillations of the flow variables. The system of linear equations derived from the finite volume procedure is solved sequentially for the velocity components, pressure correction and turbulence scalars using the strongly implicit procedure of Stone [14].

3. Results and Discussion

3.1 Computational details:

Two dimensional simulation has been carried out for the root section of the rectangular planform which is Selig-4083 mean camberline at a Reynolds number of 2.4×10^5, based on the chord length (C) of the section and wind speed of about 14 m/s. The section of the wing is a thin camberline with 1% thickness deposited and the leading edge (LE) is modeled by fitting a spline whereas the trailing edge (TE) is closed by simply joining at the mid point. Using the in-house grid generation code [15] a H-grid topology (193×63) is generated and the near wall grid spacing is so adjusted to maintain a $y+ < 3$. The third order accurate QUICK [16] scheme for convective flux discretization coupled to scalable standard $k-\varepsilon$ turbulence model [9] has been used for the present 2D computation.

Three dimensional flow simulations have been carried out for the flow past thin wing with two different planforms (rectangular and inverse-Zimmerman) having a semi-span of 0.6 C and whose cross-section is Selig-4083 cambered line with 1% thickness. The flow Reynolds number for this analysis has been fixed as 2.4×10^5 based on the root chord length (C) and wind speed of 14 m/s. For the present study a H-H grid topology with two blocks (one for the suction and other for the pressure side) covered by 193 × 63 × 69 grid points along the stream wise, normal and span wise directions respectively has been generated using the in-house grid generation code [15]. Typical view of the grid on the wing surface and the symmetry plane for the two planforms are shown in the Fig. 1. The computational domain and the boundary conditions used for the present simulation are shown in Fig. 2. Relatively coarser grid with the near wall $y+$ around 35 with the first order upwind scheme [17] for convective flux discretization coupled to standard k-ε turbulence model [9] has been used for this three dimensional analysis. The eddy viscosity at far field is assumed to be ten times of the laminar viscosity.

3.2 Three dimensional effects on the aerodynamic characteristics

The three-dimensional effects which are observed to play a prominent role for wings with low AR have been studied by comparing with the 2D simulation for the root section (Selig-4083 camberline) of the rectangular wing (AR=0.6). The aerodynamic coefficients obtained for the root section and the rectangular wing are compared and shown in Fig. 3. It is clearly evident from these plots that the aerodynamic characteristics obtained for 2D wing section is distinctly different from the rectangular wing. The 2D simulation as expected predicts a higher lift (Fig. 3(a)) and drag (Fig. 3(b)) coefficient with an early stall as compared to the 3D simulation. It is further observed that the rectangular is more stable $\left(\frac{dC_m}{d\alpha} \cong 0\right)$ when compared the 2D root section of the same wing (Fig. 3(c)). However the variation of lift-to-drag ratio (L/D) with angle of attack (α) for the 2D section and the rectangular wing are almost same except for the $(L/D)_{\max}$ which is significantly higher for the 2D case.

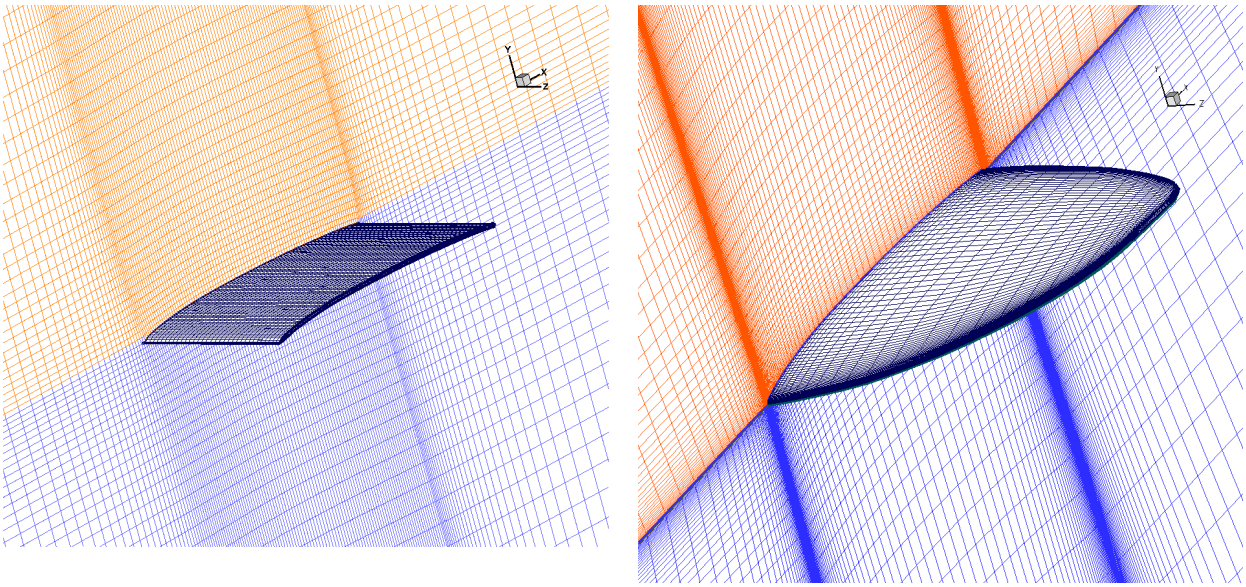

(a) Rectangular planform (b) Inverse Zimmerman planform

Fig. 1 Typical view of the grid on the symmetry plane and wing surface (AR=0.6)

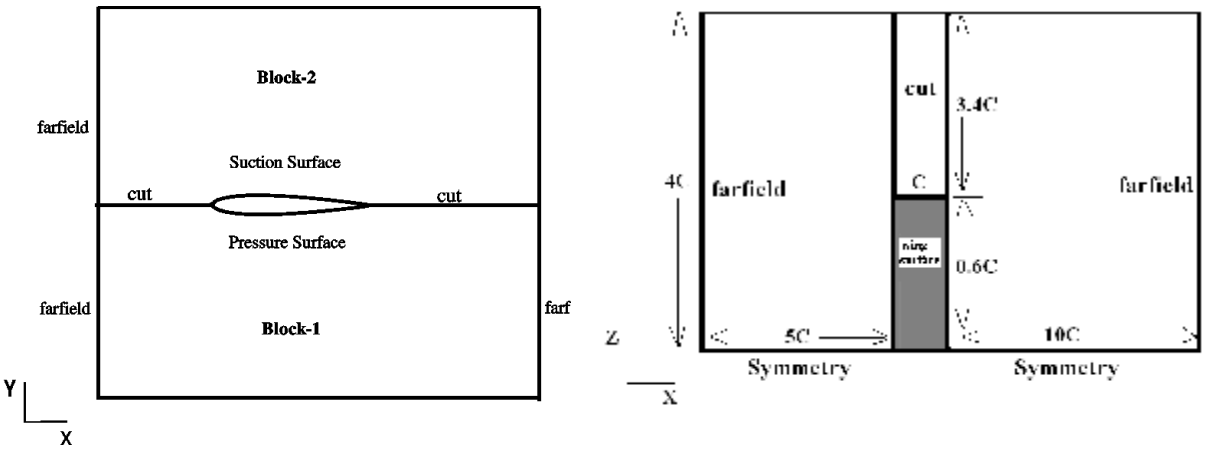

(a) Typical boundary conditions on X-Y plane (b) Typical boundary conditions on X-Z plane

Fig. 2 Boundary condition and computational domain for H-H grid topology

The computed contours of pressure coefficient, $C_p\left(=\frac{p-p_{ref}}{1/2\rho U_{ref}^2}\right)$ and particle trace are shown in Fig. 4 and Fig. 5 respectively. The value of suction and stagnation pressure obtained by the 2D simulation is almost double than that obtained by 3D simulation which justifies the higher lift coefficient obtained for the 2D wing section (see Fig. 4 and Fig. 6). For the 2D simulation the entire aerofoil is covered by a separation bubble (Fig. 5) at $\alpha=10^o$ which is consistent with the early stall prediction. On the other hand, the flow remains attached for the rectangular wing at the same angle of attack (α) with the formation of the tip vortex as shown in Fig. 8(a). This analysis has clearly indicated the strong three dimensional influence on the aerodynamic characteristics of thin wings with low AR and hence one cannot approximate the 3D wing by 2D section as typically done for higher AR in order to reduce the computational effort.

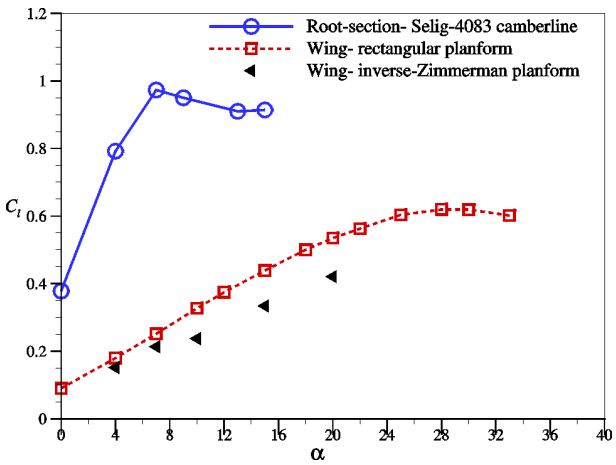

(a) Lift coefficient

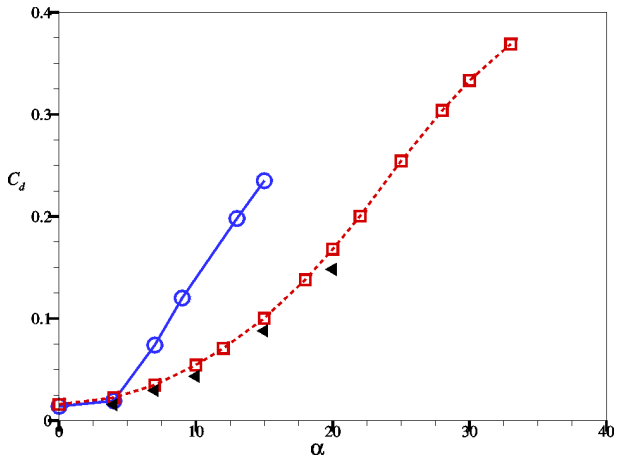

(b) Drag coefficient

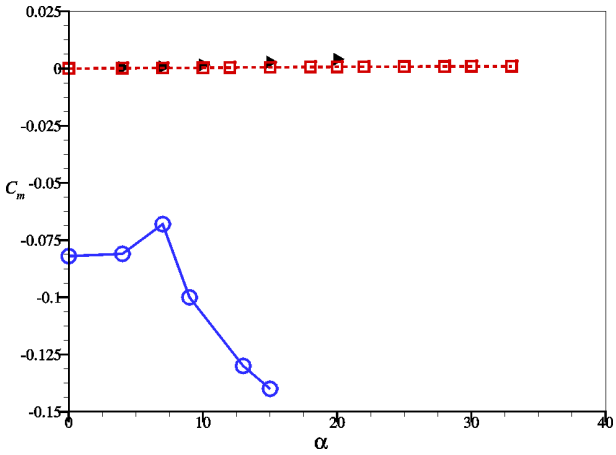

(c) Moment coefficient

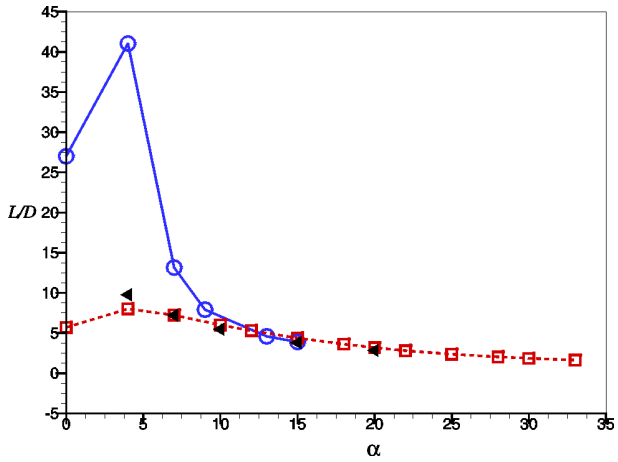

(d) Lift-to-Drag(L/D) ratio

Fig. 3 Variation of aerodynamic coefficients for wing section and wings with two different planforms ($Re=2.4\times10^5$)

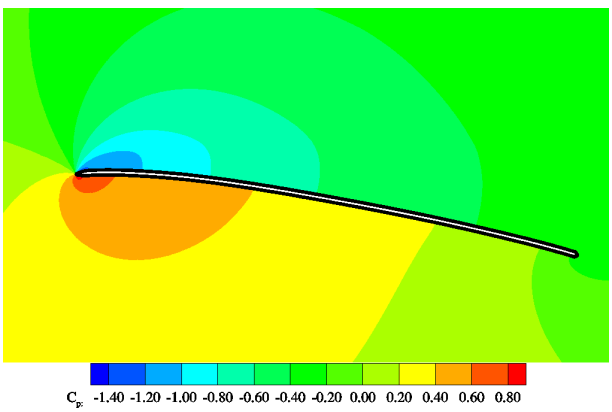

Fig. 4 Surface Contours of C_p on the root section of the wing ($Re=2.4\times10^5$, $\alpha=10^o$)

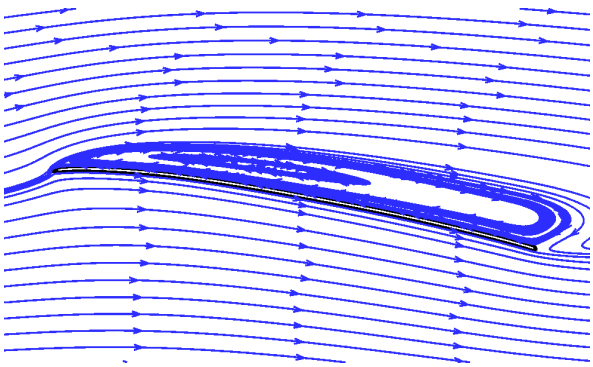

Fig. 5 Computed particle trace on the root section of the wing ($Re=2.4\times10^5$, $\alpha=10^o$)

3.3 Effect of planform on the aerodynamic characteristics

In this subsection the 3D simulations carried out for thin wings with different planforms *viz.*, rectangular and inverse Zimmerman at Re=2.4×10^5 are presented. Simulations for the rectangular planform have been carried out up to the stall (α ranging from 0^o to 35^o) where as for the wing with inverse Zimmerman planform results are currently available only for few angles of attack. Fig. 6 and Fig. 7 show the computed contours of surface pressure coefficient (C_p) on the suction and pressure side for rectangular and inverse Zimmerman planform respectively. The pressure distribution obtained is quite realistic with the rectangular wing having higher suction and stagnation pressure zones as compared to the wing with inverse Zimmerman planform. The typical streamlines computed for the two planforms at $\alpha=10^o$ are shown in Fig. 8. For both the configurations the flow is observed to remain attached on the surface of the wing and also the tip vortex has been captured reasonably well.

The aerodynamic coefficients computed for the two planforms are shown in Fig. 3. It is clearly evident from these figures that the variation of C_l with angle of attack are almost similar at lower angles of attack and deviates only at higher angles of attack with the rectangular wing having a higher lift coefficient. Further there is a small kink observed in the lift curve of the wing at around $\alpha=8^o$ which is more prominent for the wing with inverse Zimmerman planform. In the measurement data also a similar kink was observed in the C_l curve for the experiments carried out for low AR wings at low Re [7]. On the other hand, there is no significant difference observed in the variation of C_d with α for the two planforms with the wing with inverse Zimmerman planform having a lesser drag resulting in almost identical variation of lift-to-drag ratio (L/D). The maximum lift-to-drag coefficient $\left((L/D)_{\max}\right)$ for the present computation is obtained around $\alpha=5^o$ which is of the same order as obtained by the measurement [7] carried out for a different low AR wing and different Reynolds number. The simulation for the wing with inverse Zimmerman planform at higher angles of attack is in progress.

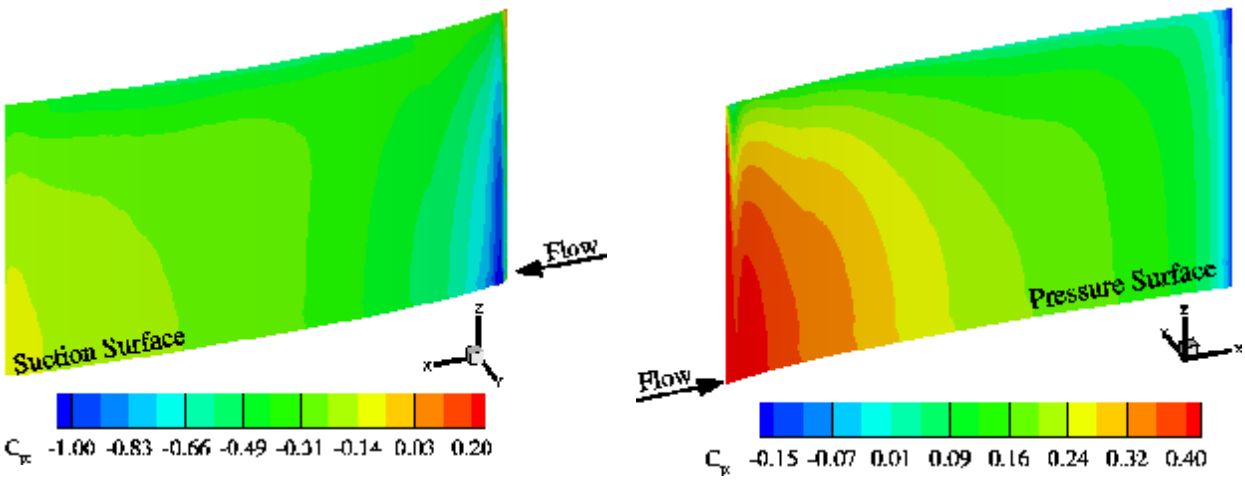

Fig. 6 Surface contours of C_p on the wing with rectangular planform ($Re=2.4\times10^5$, $\alpha = 10^o$)

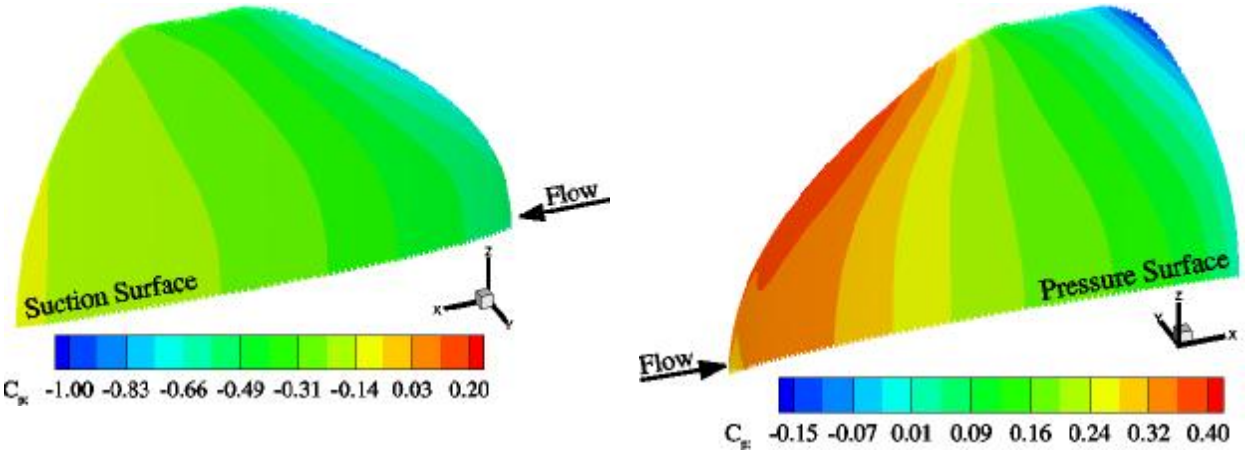

Fig. 7 Surface contours of C_p on the wing with inverse Zimmermann planform ($Re=2.4\times10^5$, $\alpha = 10^o$)

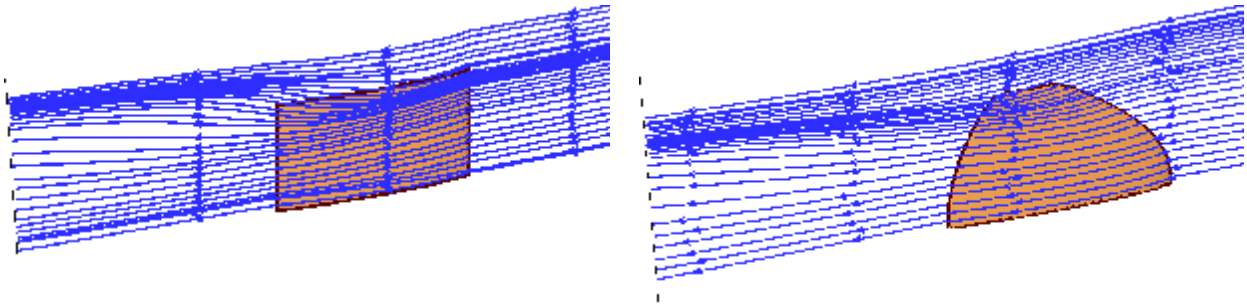

(a) Rectangular planform (b) Inverse Zimmerman planform

Fig. 8 Computed streamlines on the wing with different planforms ($Re=2.4\times10^5$, $\alpha = 10^o$)

4. Concluding Remarks

The RANS3D flow solution code has been successfully used for flow past thin low AR wings and wing section at a relatively low Reynolds number (Re=2.4×10^5) in order to study the effect of three dimensional flow and different planform shapes on the aerodynamic characteristics. The realistic flow characteristics obtained by the present simulations confirms the adequacy of the mathematical modeling and the numerical accuracy of the RANS3D code. Due to the non availability of the measurement data for the present wing configuration and Reynolds number, the results obtained by this computations have been compared with the measurement for a different low AR wing and different Re (10^5) and found to agree reasonably well with measurement data in a qualitative sense. Further analysis will be carried out for the wing using higher order spatial discretization schemes as well as finer grid resolution especially in the boundary layer and near the wing tip. Work is in progress to incorporate the correlation based transition model in the RANS3D code.

5. Acknowledgement:

The authors wish to thank Director NAL and Head CTFD Division, NAL Bangalore for permitting us to publish this paper. The authors also wish to express their heartfelt thanks to project assistants Mr. Pradeep Shetty and Mr. G. Bhanu Kishan for their support in preparing this paper.

References

[1] J. M. Grameyer and M. T. Keennon., "Development of the black Micro Air Vehicle". *AIAA Paper,* No. 2001-0127, 2001

[2] P. J. Kunz. "*Aerodynamics and design for ultra-low Reynolds number flight"* . PhD Dissertation, Stanford University, US, 2003

[3] E. J. Schroeder., "*Low Reynolds number flow validation using Computational Fluid Dynamics with application to Micro Air Vehicles",* Master of Science Dissertation, Department of Aerospace Engineering, University of Maryland, US, 2005.

[4] G. W. Jones, C. J. Bradshaw, J. Papadapoulos, and M. F. Paltzer., "Improved performance and control of flapping-wing propelled Micro Air Vehicles", *AIAA Paper*, No. 2004-0399, 2004.

[5] W. Shyy, M. Berg, and D. Ljungqvist., "Flapping and flexible wings for biological and micro vehicles*", Progress in Aerospace Sciences*, Vol. 35, No. 5, pp 455–506, 1999.

[6] B. R. Hein., "Hover performance of a Micro Air Vehicle: Rotors at low Reynolds number", *AHS Lichten Award Competition*, 2005.

[7] T. J. Mueller, "*Fixed and flapping wing aerodynamics for micro air vehicles applications*", Vol.195, Progress in Astronautics and Aeronautics, edited by T. J Mueller and published by AIAA , 2001

[8] R. T. Jones., "*Wing Theory",* Princeton University Press, 1990.

[9] B. E. Launder and D. B. Spalding, "The Numerical Computation of Turbulent Flows", *Computer Methods in Applied Mechanics & Engineering*, Vol. 3, No. 2, pp. 269-289, March 1974.

[10] S. Majumdar, W. Rodi, and J. Zhu, "Three dimensional finite volume method for incompressible flows with complex boundaries", *Jl. of Fluids Engineering*, Vol. 114, No. 4, pp. 496–503, 1992.

[11] S. Majumdar, B. N. Rajani, D. S. Kulkarni and M. B. Subrahmanya, "CFD Simulation of Low Speed Turbulent Flow Problems Using Unsteady RANS and Large Eddy Simulation Approach", *Jl. of Aerospace Sciences and Technologies*, Vol. 61, No. 1, pp. 111 – 122, February 2009.

[12] S. V. Patankar and D. B. Spalding., "A calculation procedure for heat,mass and momentum transfer in three dimensional parabolic flows", *International Jl. of Heat and Mass Transfer*, 15:1787–1806, 1972.

[13] S. Majumdar., "Role of underrelaxation in momentum interpolation for calculation of flow with non-staggered grids", *Numerical Heat Transfer*, No. 13, 125–132, 1988.

[14] H. L. Stone., "Iterative solution of implicit approximations of multidimensional partial differential equations", *SIAM Jl. of Numerical Analysis*, Vol. 5, pp 530–530, 1968.

[15] A. Fathima, N. S. Baldawa, S. Pal and S. Majumdar, "Grid generation for arbitrary 2D configurations using a differential algebraic hybrid method", *NAL Project Document CF9416*, 1994

[16] B. P. Leonard, A stable and accurate convective modelling procedure based on quadratic upstream interpolation, *Computer Methods in Applied Mechanics & Engineering*, Vol. 19, No. 1, pp 59–98, 1979.

[17] D. S. Kulkarni, B. N. Rajani and S. Majumdar, "Studies on temporal and special discretization schemes used in pressure based RANS algorithm for incompressible flow", *NAL Project Document CF0108*, 2001.